PAPER

Check for updates

Facilitated electron transfer by Mn dopants in 1-dimensional CdS nanorods for enhanced photocatalytic hydrogen generation†

Walker MacSwain, [a] Hanjie Lin,[a] Zhi-Jun Li, [a] Shuya Li,[a] Chun Chu,[a] Lacie Dube,[b] Ou Chen,[b] Gyu Leem [cd] and Weiwei Zheng *[a]

Using sunlight to produce hydrogen gas *via* photocatalytic water splitting is highly desirable for green energy harvesting and sustainability. In this work, Mn^{2+} doped 1-dimensional (1D) CdS nanorods (NRs) with Pt tips (*i.e.*, 1D Mn:CdS-Pt NRs) were synthesized for photocatalytic water splitting to generate hydrogen gas. The incorporation of Mn^{2+} dopants inside the 1D CdS NRs with a significantly longer lifetime (~ms) than that of host excitons (~ns) facilitates charge separation; the electron transfer to metal Pt tips leads to enhanced photocatalytic activity in water splitting redox reactions. The as-synthesized Mn^{2+} doped CdS NR-based photocatalyst generated an order of magnitude greater yield of hydrogen gas compared to the undoped CdS NR-based photocatalyst. The enhanced charge transport from the long lifetime excited state of Mn^{2+} dopants in light harvesting semiconductor nanomaterials presents a new opportunity to increase the overall photocatalytic performance.

Introduction

Photocatalytic hydrogen generation by water splitting has drawn a tremendous amount of research interest due to its green nature and promising solution for the world energy crisis.[1] Quantum confined semiconductor nanocrystals (NCs) have excellent optical and electrical properties including a large absorption extinction coefficient in the visible range, size- and shape-tunable bandgap, and great photostability. The photo-generated charge carriers (*i.e.*, excited electrons and holes) from NCs can be used for photocatalytic redox reactions, such as photocatalytic water splitting for hydrogen generation. To date, there are multiple semiconductors including metal chalcogen-ides such as CdS,[2,3] CdSe,[4–6] and PbS,[7] and metal oxides such as ZnO[8] and TiO_2[9] that have been developed to split water and generate hydrogen gas. Among these materials, CdS NCs have

been heavily utilized due to their ~2.4 eV bandgap, which is narrow enough to absorb visible light while still having a conduction band that is sufficiently negative to reduce water to produce hydrogen gas.[3,10,11] However, the photocatalytic yields of CdS NCs are limited primarily due to insufficient charge separation as a result of fast exciton recombination (on the order of ns to tens of ns) compared to slower surface cata-lytic reactions (ms to s).[11–14] The insufficient charge separation leads to limited charge carriers (electrons and holes) accessible to photocatalytic redox reactions.

Increased photocatalytic yields of water splitting for H_2 gas generation have been reported from 0-dimensional (0D) CdS QDs of 17 (μmol h^{-1} g^{-1})[15] to 1D CdS nanorods (NRs) of 60 (μmol h^{-1} g^{-1}),[16] while 2D CdS nanoplatelets have been reported to have 30.3 (μmol h^{-1} g^{-1}),[17] tetrapods ~2640 (μmol h^{-1} g^{-1}),[18] cubes 1600 (μmol h^{-1} g^{-1}),[19] and pyramids 4600 (μmol h^{-1} g^{-1}).[18] These increases in reaction yields are due to the slight polarizations when exciting electrons across the unconfined axis or axes, leading to a reduced charge recombination rate.[20] Therefore, advanced shaped CdS NCs with enhanced charge separations can increase the efficiency of photocatalytic redox reactions including water splitting.[12,17,21] Another approach to increasing the charge separation in CdS NCs is by adding a metal co-catalyst, such as Pt,[12,17,21–23] Au,[24,25] Ni,[6,26,27] and Ag,[28] with efficient electron transfer from CdS to the metal co-catalyst. The metal co-catalyst acts as a sink for the excited electrons to move into which can increase the charge separation due to a fast rate of electron transfer (~ps)[25] from the conduction band of CdS to the metal.

Pt nanoparticles (NPs) are widely used as co-catalysts in CdS-based photocatalytic water splitting[12,17,22,23,29] since Pt can both

ᵃDepartment of Chemistry, Syracuse University, Syracuse 13244, New York, USA. E-mail: wzhen104@syr.edu

ᵇDepartment of Chemistry, Brown University, Providence, 02912, Rhode Island, USA

ᶜDepartment of Chemistry, State University New York College of Environmental Science Forestry, Syracuse 13210, New York, USA

ᵈThe Michael M. Szwarc Polymer Research Institute, 1 Forestry Drive, Syracuse 13210, New York, USA

† Electronic supplementary information (ESI) available: Experimental details for ZnS shell coated core/shell NRs, characterization data (TEM and XRD), optical data (absorbance, emission, and PL lifetime), electrochemical data (EIS, CV, photocurrent, and band edge), quantum efficiency calculations, band structures for Mn:CdS/ZnS, and control experiments of photocatalysis (recycle test, doping concentration and Pt NP size-dependent photocatalytic performance). See DOI: https://doi.org/10.1039/d2ta08409k

readily accept electrons into its Fermi energy level and is highly hydrophilic. This innate hydrophilicity increases the possibilities of hydrogen adsorption on the active sites of the Pt co-catalyst, which can increase the likelihood of an excited electron being involved in photocatalytic water splitting for hydrogen gas generation. Coupled with a light harvesting CdS NC photocatalytic system, Pt co-catalysts have shown significantly higher hydrogen yields among the available co-catalysts.[12,17,21,23,29,30] For example, the photocatalytic water splitting yield of Pt modified CdS NCs has been reported to be 56 000 (μmol h^{-1} g^{-1}),[30] while other CdS-based metal co-catalysts have reported 400.6 (μmol h^{-1} g^{-1}) for Au,[24,25] 25 484 (μmol h^{-1} g^{-1}) for Ni,[26] and 32 (μmol h^{-1} g^{-1}) for Ag.[28]

However, changing the dimensionality of the CdS photocatalyst and adding a Pt co-catalyst cannot completely overcome the issue of inherent short lifetimes of excitons ($\sim$ns) even though a portion of charge carriers can transport to the Pt particles before exciton recombination. Doping transition metal ions inside the host semiconductor lattice can provide an additional exciton relaxation pathway by host-to-dopant energy transfer; this is an attractive strategy for increasing catalytic performance as the dopants can alter the dynamics of charge separation and recombination.[27,31–34] Manganese (Mn^{2+}) ions are a particularly useful dopant as their orange emission around 600 nm has a long emission lifetime ($\sim$ms) from the spin forbidden d–d transition ($^4T_1$ to $^6A_1$).[31,33–37] The ms lifetime of the excited state of Mn^{2+} dopants is much longer (4–6 orders of magnitude higher) than that of the fast decay of excitons of semiconductor NCs (on the order of ns or tens of ns). Therefore, the long lifetime Mn^{2+} dopants can provide a much longer time frame for charge transport[38] or energy transfer,[39] which is on a similar order of magnitude to surface photocatalytic reactions (ms–s).[13,14] Previous studies have demonstrated that doping Mn^{2+} into 0D CdS QDs increases the photocatalysis yield of hydrogen gas from 17 (μmol h^{-1} g^{-1})[15] in the undoped system to 300 (μmol h^{-1} g^{-1}).[38] Therefore, greater charge separation can occur by host-to-dopant energy transfer which can increase the photocatalytic yield.

In this report, we designed a new photocatalyst by doping Mn^{2+} ions into 1D CdS NRs with Pt-tips (i.e., 1D Mn:CdS-Pt NRs) for photocatalytic H$_2$ generation from water splitting (Fig. 1).
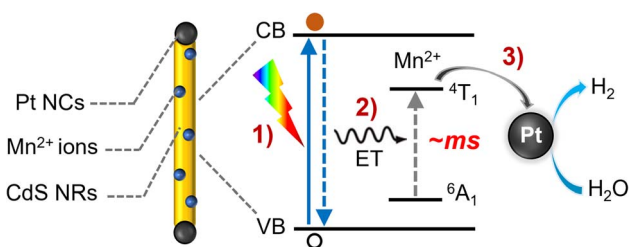
Following photoexcitation of host CdS NRs to generate excited electrons and holes (step 1 in Fig. 1), two-step charge carrier transport occurs including host-to-dopant energy transfer (step 2 in Fig. 1) and electron transfer from Mn^{2+} dopants to Pt NPs (step 3 in Fig. 1). The added charge transport pathways mediated by the long lifetime dopants could prevent the fast exciton recombination, leading to enhanced photocatalytic water splitting. Aided by the 4.1 ms Mn^{2+} dopant emission lifetime, compared to the 7.9 ns lifetime of the host 1D CdS NRs, the Mn^{2+} doped 1D CdS NRs can efficiently boost the charge separation and the following electron transportation for photocatalytic water splitting under blue light irradiation. Compared with their undoped counterpart (i.e., 1D CdS-Pt NRs), the water splitting efficiency of Mn:CdS-Pt NRs increased from 64 000 to 287 000 μmol h^{-1} g^{-1} of hydrogen gas; the yield is increased by 448% ($\sim$4.5-fold enhancement). The long lifetime of the dopants can increase charge separation and supply a bridging pathway for efficient photocatalysis on metal co-catalysts, which provide a new opportunity for photocatalytic redox reactions.

Experimental section

Chemicals

Cadmium oxide (CdO, $\geq$99.0%, Sigma Aldrich), sulfur (99.998%, Sigma Aldrich), 1-tetradecylphosphonic acid (TDPA, 98%, Sigma Aldrich), trioctylphosphine oxide (TOPO, 99%, Alfa-Aesar), trioctylphosphine (TOP, 90%, Sigma Aldrich), chloroform (99.8%, Fisher Scientific), Mn(II) acetate anhydrous (99.99%, Alfa-Aesar), oleylamine (OAm, 70%, Sigma Aldrich), oleic acid (OA, 90%, Sigma Aldrich), 1, 2-dichlorobenzene ($\geq$99%, Sigma Aldrich), diphenyl ether ($\geq$99%, Sigma Aldrich), 1, 2-hexanedecanediol (90%, Sigma Aldrich), 3-mercaptopropionic acid (MPA, 99%, Alfa Aesar), tetramethylammonium hydroxide (TMaOH, 98%, Alfa Aesar), platinum(II) acetylacetonate ($\geq$99.98%, Sigma Aldrich), methanol ($\geq$99%, VWR), toluene ($\geq$99.5%, EMD Chemicals), ethanol ($\geq$99%, anhydrous, Pharmco), acetone ($\geq$99.5%, Sigma Aldrich), ethyl acetate ($\geq$99%, ACROS), hexane (99%, EMD), isopropyl alcohol (IPA $\geq$99.5% Sigma Aldrich), and potassium hydroxide ($\geq$85%, Sigma Aldrich). All chemicals were used as purchased without further purification.

Synthesis of 1D CdS NRs

1D CdS NRs were synthesized based on a slightly modified method from the literature.[40] Cadmium and sulfur precursor solutions were first prepared separately. The cadmium precursor solution was prepared by mixing 115 mg (0.9 mmol) CdO, 415 mg (1.5 mmol) TDPA, and 3.5 g TOPO in a 50 mL flask and degassing for 1.5 h at 80 °C. The flask was then heated to 340 °C under an Ar flow to form a Cd-TDPA complex indicated by a change in the solution color from dark red to optically clear and then cooled to 300 °C. The sulfur precursor solution (S-TOP solution) was prepared by dissolving 110 mg (3.4 mmol) of sulfur powder in 10 mL of degassed TOP.

For a typical synthesis of 1D CdS NRs, 3 mL of the room temperature S-TOP precursor solution was injected into the hot

Fig. 1 Schematic illustration of the excitonic and energy transfer processes in Mn^{2+} doped CdS NRs with Pt-tips for H$_2$ generation. (1) Photoexciting an electron from the valence band (VB) to the conduction band (CB), (2) energy transfer (ET) from the host CdS NR to Mn^{2+} dopants, and (3) electron transfer from dopants (with $\sim$ms lifetime) to active sites of Pt NP tips for H$_2$ generation from water splitting.

This journal is © The Royal Society of Chemistry 2023

J. Mater. Chem. A, 2023, **11**, 7066–7076 | **7067**

Cd-TDPA solution at 300 °C, and the temperature of the reaction mixture dropped after addition, and then ramped back to 300 °C in ~10 min. The remaining S-TOP (~7 mL) solution was injected, 1 mL at a time, every 5 minutes over a 35 minute period, and the reaction then proceeded for an additional 30 minutes. At the end of the reaction, the solution was removed from the heating mantle and allowed to cool to approximately 60 °C and then 2–3 mL of chloroform was added to prevent solidification of the crude solution. The CdS NRs were separated from the crude solution by precipitating the particles with ethanol and centrifuging, and then dispersed in hexane for optical measurements. The precipitate was further purified once by resuspending the NRs in toluene and then reprecipitating with ethanol and centrifuging.

Synthesis of 1D Mn:CdS NRs

The Mn^{2+} dopant precursor ($Mn(S_2CNEt_2)$) was synthesized by adding 96 mg (0.56 mmol) of NaS_2CNEt_2 to a flask and vacuumed to remove air and moisture and then refilled with Ar gas. Inside a glovebox, typically, 63 mg (0.36 mmol) of Mn(II) acetate anhydrous and 1 mL of TOP were added to the NaS_2CNEt_2 flask. Then the solution was placed under vacuum and heated to 110 °C for further use.

The synthesis of Mn:CdS NRs followed a similar procedure used for CdS NRs except dropwise addition of the 1 mL $Mn(S_2CNEt_2)$ precursor into Cd-TDPA solution at 300 °C, before S-TOP injection, and allowed to settle for ~10 minutes. In addition, 9 mL S-TOP was used (instead of 10 mL S-TOP used in the synthesis of CdS NRs to keep the total volume of the TOP in the reaction solution the same as the undoped CdS NRs) with 2.7 mL of S-TOP injected in the first step followed by injecting 0.9 mL every 5 minutes, and the reaction then was allowed to proceed for an additional 30 minutes. The same purification method was used as for the undoped CdS NRs.

Synthesis of Pt NP tipped 1D Mn:CdS-Pt NRs

Pt NP tipped 1D NRs were synthesized based on a slightly modified method from the literature.[41] First, OA (0.2 mL), OAm (0.2 mL), and 43.0 mg of 1,2-hexadecanediol (0.17 mmol) were heated in diphenyl ether (9 mL) in a 25 mL three-neck flask at 80 °C under vacuum for 30 min to remove the trace amount of water and air. The optical density (OD) of the CdS-based NR stock solution was measured by diluting the stock solution of NRs (100 μL into 1 mL i.e., 100× dilution) and the OD of the NR stock solution can be calculated from the absorbance of the diluted solution multiplied by 100. 65.5 mg (0.17 mmol) Pt(II) acetylacetonate was added to the suspension of the synthesized CdS or Mn:CdS NRs (stock solution OD = 20) in 3 mL of 1, 2-dichlorobenzene and sonicated at 65 °C for 10 min to promote the dissolution of the Pt precursor. The reaction mixture was purged with Ar and heated to 200 °C before injecting the 3 mL suspension of the Pt precursor and NRs. Typically, after 10 minutes the reaction mixture was removed from heat and quenched in a water bath. The product was washed by precipitation in ethanol followed by centrifugation. The precipitate was further purified twice by resuspending the NRs in hexane and then reprecipitating with ethanol and centrifuging before ligand exchange.

Ligand exchange

To make water soluble NRs, MPA ligand exchange was performed. An excess amount of MPA (1 mL) was dissolved in 5 mL methanol and the pH of the solution was adjusted to above 12 with TMaOH. The as-synthesized NRs (typically 0.23 mmol) were dispersed in 5 mL hexane and added to the above 6 mL MPA ligand solution in methanol. The solution was stirred overnight in aluminum foil wrapped containers. The MPA capped NRs were precipitated with ethyl acetate and isolated by centrifugation. The precipitate was further purified once by resuspending the NRs in methanol and then reprecipitating with ethyl acetate and centrifuging.

Sample characterization

Powder X-ray diffraction (XRD) patterns were taken on a Bruker D2 Phaser with a LYKXEYE 1D silicon strip detector using Cu K_{α} radiation (λ = 1.5406 Å). Transmission electron microscopy (TEM) images and high-resolution (HR) TEM images were obtained on a JEM 2100F TEM (operated at an accelerating voltage of 200 kV). UV-visible (UV-vis) absorption measurements were collected on an Agilent Cary 60 spectrophotometer. Photoluminescence (PL) measurements were performed with a Horiba FluoroMax Plus spectrofluorometer. Time-resolved emission measurements were conducted using an Edinburgh FLS-980 spectrometer with a photomultiplier tube (PMT, R928 Hamamatsu) detector. For CdS NR bandgap PL lifetime measurements, pulsed excitation light was generated by using an Edinburgh EPL-365 pulsed laser diode at a repetition rate of 0.2 MHz. For Mn^{2+} emission lifetime measurements, pulsed excitation light was generated by using an μF2 60 W xenon flashlamp operating at a repetition rate of 20 Hz. Elemental composition analysis was performed on a PerkinElmer Avio 220 Max inductively coupled plasma-optical emission Spectrometer (ICP-OES). X-ray photoelectron spectroscopy (XPS) analysis was performed using a Thermo Scientific KAlpha+ instrument operating under Al K_{α} radiation (1486.6 eV). All XPS spectra were calibrated by using the carbon 1s peak at 284.8 eV. Room-temperature X-band EPR spectra were recorded on a Bruker ELEXSYSII E500 spectrometer at a microwave frequency of 9.8 GHz. For cyclic voltammetry (CV), electrochemical impedance spectroscopy (EIS), and photocurrent measurements, a Gamry Interface 1010E electrochemical workstation was used, and the measurements were performed with a single three-electrode setup with the sample electrode as the working electrode, a platinum wire as the counter electrode, and Ag/AgCl (0.1 M $NaClO_4$, $E_{Ag/AgCl}$ = +0.194 V vs. NHE) as the reference electrode. EIS was performed in 0.1 M $NaClO_4$ at 1.0 V vs. NHE with an amplitude of 25 mV (frequency: 100 mHz–100 kHz). The electrochemical electrolyte was degassed for 30 min by flushing with high purity argon prior to CV and EIS measurement. Photocurrent tests were performed in 0.1 M $NaClO_4$ at 0.3 V vs. NHE with a 405 nm LED.

7068 | J. Mater. Chem. A, 2023, **11**, 7066–7076

This journal is © The Royal Society of Chemistry 2023

Photocatalytic water splitting for generating hydrogen gas

250 μL (0.009 mg) MPA-ligand exchanged NRs in distilled water (stock solution OD = 26) were added to a 15 mL glass centrifuge tube with a stir bar and 2.25 mL distilled water. To each reaction tube, 500 μL of 0.1 M KOH was added to adjust the pH to $\geq$ 12 and 2.5 mL of isopropyl alcohol was added as a sacrificial hole scavenger. The sample solutions were then vacuumed and refilled with Ar gas. The photochemical reactions were performed in a photochemical reactor equipped with 405 nm LEDs ($\lambda_{max} = 405 \pm 15$ nm) under stirring at 1000 rpm. The volume of the generated H_2 gas was collected in a burette and recorded every 15 or 30 minutes.

Results

1D Mn:CdS-Pt NRs

In this study, we synthesized Mn^{2+} doped 1D CdS NRs with Pt NP tips (*i.e.*, Mn:CdS-Pt NRs) to study the role of dopants and the metal co-catalyst on the photocatalytic performance. Firstly, 1D Mn:CdS NRs were synthesized *via* a hot-injection method by injecting the S-precursor into the Cd and Mn-precursor in trioctylphosphine/trioctylphosphine oxide (TOP/TOPO) solution at 300 °C. Undoped CdS NRs were also synthesized for comparison with the same procedure without adding the Mn-precursor in the reaction. The as-obtained Mn:CdS NRs were then tipped with Pt by reduction of Pt in diphenyl ether with 1,2 hexadecanediol at 200 °C (see details in the Experimental section).

The structure and morphology of the 1D CdS NR-based photocatalysts were characterized by XRD and TEM. The XRD patterns of the undoped and Mn^{2+} doped CdS NRs, as well as the Mn:CdS-Pt NRs, indicate hexagonal phase CdS in these 1D NRs (Fig. 2a).[42,43] Compared with the standard hexagonal CdS XRD pattern, the (002) diffraction peak is obviously intensified, indicating cylindric growth for non-spherical NCs along the [001] direction (perpendicular to the (002) plane). The TEM images (Fig. 2b and c) of the as-synthesized products show both CdS and Mn:CdS to be 1D cylindrical NRs with an average diameter of 4.1 $\pm$ 0.3 nm and 4.2 $\pm$ 0.3 nm, and an average length of 52 $\pm$ 5.0 nm and 50 $\pm$ 5.0 nm, respectively. The TEM images and histogram analysis (Fig. S1a–d†) show no significant difference in the diameter and length of the 1D NRs despite the addition of Mn^{2+} dopants. After adding Pt at the tips of Mn:CdS NRs, a new XRD peak is present at 39.7°, which can be assigned to the (111) plane of Pt (indicated as ★ in Fig. 2a).[41] The TEM image of the Mn:CdS-Pt NRs indicates small, dark Pt NPs with an average diameter of 4.4 $\pm$ 0.5 nm tipped at both ends of the CdS NRs with a "dumbbell" type shape (Fig. 2d). The average diameter of Mn:CdS in Mn:CdS-Pt NRs is 4.1 $\pm$ 0.3 nm and the average total length, including the Pt tips, is 58 $\pm$ 5.0 nm (Fig. S1e and f†). The slightly longer Mn:CdS-Pt NRs, compared to the NRs without the Pt tips, are consistent with the addition of the two Pt NPs on each end of the NRs (Fig. S1f and g†). The HR-TEM image of Mn:CdS-Pt NRs (Fig. 2e and f) shows a lattice fringe of 3.3 Å from the (002) plane of hexagonal CdS NRs and a lattice fringe of 2.3 Å from the (111) plane of a face-centered cubic (fcc) Pt lattice (Fig. 2f).
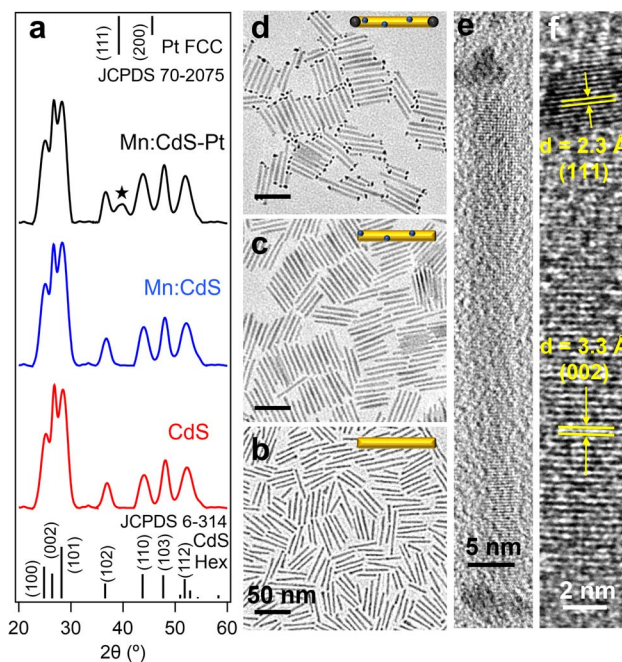

Fig. 2 (a) The powder XRD patterns of 1D CdS, Mn:CdS, and Mn:CdS-Pt CdS-based NRs (★ indicates the diffraction peak from Pt). TEM images of (b) CdS NRs, (c) Mn:CdS NRs, and (d) Mn:CdS-Pt NRs; HR-TEM images of (e) a Mn:CdS-Pt NR and (f) a portion of a Mn:CdS-Pt NR showing the d spacing of 3.3 Å and 2.3 Å of the (002) plane of the CdS NR and the (111) plane of the Pt NP tip, respectively.

The survey XPS spectrum (Fig. 3a) of the Mn:CdS NRs shows distinct peaks for Cd 3d, S 2s, and Mn 2p. For the untipped Mn:CdS NRs, the Mn^{2+} dopant peak is at 653.5 eV ($2p_{1/2}$) (Fig. 3b), the S 2p peaks are at 163.1 eV ($2p_{3/2}$) and 164 eV ($2p_{1/2}$) (Fig. 3c), and the Cd 3d peaks are at 406.5 eV ($3d_{5/2}$) and 413.3 eV ($3d_{3/2}$) (Fig. 3d), which is consistent with the literature reported
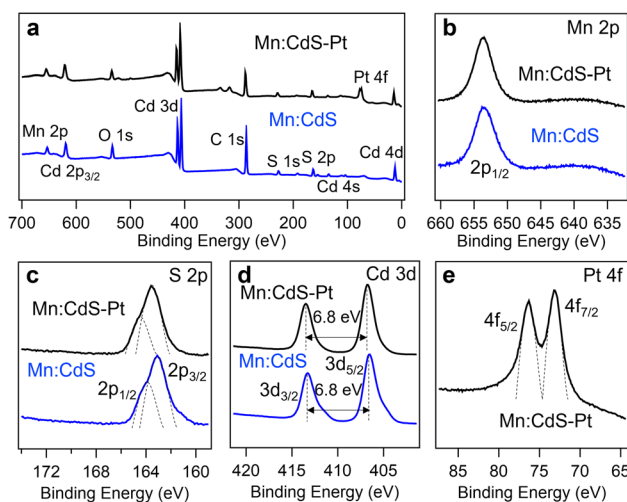

Fig. 3 X-ray photoelectron spectroscopy (XPS) of 1D Mn:CdS and Mn:CdS-Pt NRs, where (a) is the survey spectrum, and the spectra of (b) the Mn 2p orbitals, (c) the S 2p orbitals, (d) the Cd 3d orbitals, and (e) the Pt 4f orbitals.

This journal is © The Royal Society of Chemistry 2023

J. Mater. Chem. A, 2023, **11**, 7066–7076 | **7069**

values.[44,45] For the Mn:CdS-Pt NRs, similar peaks were observed for Mn, Cd, and S with a new peak present for Pt 4f at 73.2 eV ($4f_{7/2}$) and 76.3 eV ($4f_{5/2}$), which are also consistent with literature reported values.[46] The Mn, Cd, and S peaks exhibit a small peak shift towards higher binding energy (0.2 eV for Mn $2p_{1/2}$, 0.3 eV for Cd $3d_{5/2}$ and $3d_{3/2}$, and 0.5 eV for S $2p_{3/2}$) in the XPS spectra when compared to the Mn:CdS NRs, which indicates that the electrons in both the CdS host CB and the Mn^{2+} dopant energy level are interacting with the Fermi level of Pt. In addition, the distance between the Cd $3d_{5/2}$ and Cd $3d_{3/2}$ peaks stays consistent at 6.8 eV, so the shift of the peak position is due to Fermi level equilibration occurring as electrons transfer from the Mn:CdS NRs to Pt.[47,48]

Optical properties

The absorption and photoluminescence (PL) spectra for the 1D CdS, Mn:CdS, and Mn:CdS-Pt NRs (Fig. 4a) show the first exciton absorption peak at ∼470 nm, from CdS, for all NRs. For CdS and Mn:CdS NRs, the CdS bandgap PL is at 480 nm and has a broad defect emission peak centered around ∼650 nm, with PL quantum yields (QYs) of 7.4% and 6.7%, respectively. There is no clear Mn^{2+} emission (usually around 600 nm) present in the Mn:CdS NRs, which might be due to the large number of surface trapping states considering the large surface to volume ratio of 1D NRs.[49] However, the Mn^{2+} PL peak at 600 nm can be observed after ZnS surface passivation (i.e., 1D Mn:CdS/ZnS NRs) to remove the surface defects (Fig. S2†). The wider

bandgap ZnS shell was chosen to form CdS/ZnS type I core/shell NRs to completely confine the electrons and holes within the CdS core, and therefore the PL spectra are not sensitive to the surface defects of NRs (see the detailed energy levels of dopants and surface defects, and the band alignment of the type I CdS/ZnS structure in Fig. S3†).[39,49–52] Furthermore, despite the lack of obvious Mn^{2+} emission, ICP-OES measurements indicate 0.9% Mn^{2+} dopant concentration in the Mn:CdS NRs, which corresponds with ∼110 Mn^{2+} ions per NR. Upon the addition of Pt to the tips of the NRs, a loss of most of the emission features was observed and the PL QY decreases to 0.9% due to the charge transfer from Mn:CdS NRs to metal Pt NP tips (Fig. 4a).

The calculated lifetimes for the CdS PL of the NRs are shown in Fig. 4b with 7.9 ns for CdS, 3.8 ns for Mn:CdS, and 1.4 ns for Mn:CdS-Pt NRs (Fig. 4b and inset). Compared with CdS NRs, the shorter lifetime of the band edge PL from Mn:CdS NRs can be attributed to the host to Mn^{2+} dopant energy transfer as an added electron relaxation pathway. Further significant decrease in the CdS PL lifetime after the Pt NPs are tipped onto the NRs occurs, which is consistent with the electron transfer from the excited states of Mn:CdS NRs to the Fermi energy level of Pt NCs. To prove the electron transfer from the Mn^{2+} dopants to the Pt NP cocatalyst, the Mn^{2+} emission lifetime of Mn:CdS/ZnS and Pt tipped Mn:CdS/ZnS NRs (i.e., 1D Mn:CdS-Pt/ZnS NRs) was measured. The Mn^{2+} emission lifetime from Mn:CdS/ZnS core/shell NRs was found to be 4.1 ms, which dramatically decreased to 0.29 ms after introducing the Pt NP tips on the Mn:CdS-Pt/ZnS NRs (Fig. 4c), indicating electron transfer from the excited states of Mn^{2+} dopants to the Fermi energy level of Pt NCs. The lifetime of the broad emission at 600 nm for CdS and Mn:CdS NRs without shell passivation was also measured to be 6.9 μs and 7.5 μs, respectively. The slightly longer lifetime of the broad emission in Mn:CdS NRs might be due to the combination of defect emission (∼μs) and Mn^{2+} emission (∼ms) (Fig. S4†).

The presence of Mn^{2+} dopants within the CdS host lattice was further confirmed by X-band EPR spectroscopy (Fig. 4d). In the Mn:CdS and Mn:CdS-Pt NRs, there are two sets of six-peak hyperfine splitting patterns with hyperfine constants (A) of 94 and 73 G, corresponding to the Mn^{2+} ions on the surface and the core of the CdS lattice, respectively, indicating random distribution of Mn^{2+} dopants in the CdS NR lattice.[49,53,54] The EPR of the Mn:CdS/ZnS NRs (Fig. 4d) only shows a singular hyperfine peak splitting pattern of 70 G from the core Mn^{2+} dopants. The dismissal of the larger EPR hyperfine splitting (94 G) after shell coating further proves that the larger and smaller EPR hyperfine splitting patterns (94 and 73 G) from the Mn:CdS NRs are from the surface and core Mn^{2+} dopants, respectively.
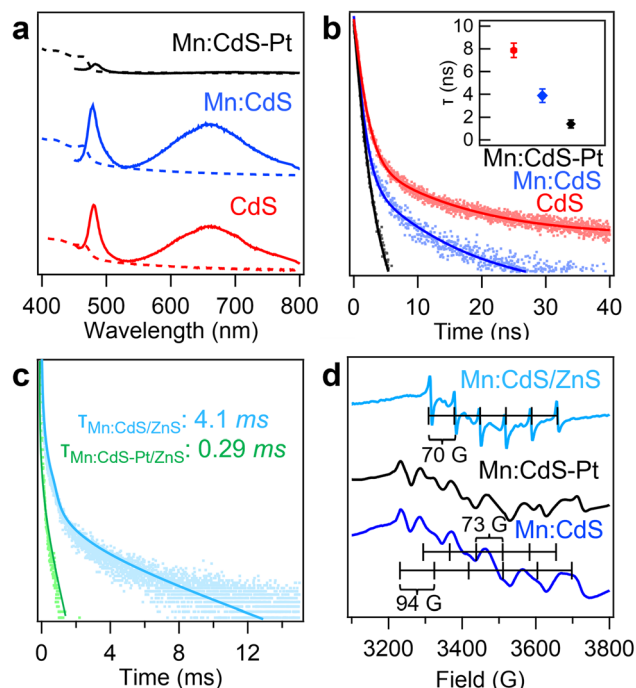

Fig. 4 (a) Absorbance (dashed lines) and PL spectra (solid lines) of CdS, Mn:CdS, and Mn:CdS-Pt NRs. (b) PL decays of the CdS emission for CdS, Mn:CdS, and Mn:CdS–Pt NRs. Inset show the calculated lifetimes (τ) in ns. (c) Mn^{2+} lifetime from core/shell Mn:CdS/ZnS and Mn:CdS-Pt/ZnS NRs. (d) Room-temperature X-band EPR spectra of Mn:CdS, Mn:CdS-Pt, and Mn:CdS/ZnS NRs.

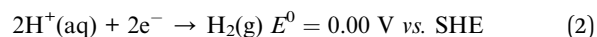## Electrochemical properties

To further confirm the role of the long lifetime Mn^{2+} dopant ions in mediating the efficient electron transport from host CdS NRs to Pt co-catalysts, the charge transport properties of the CdS-based NRs were studied by electrochemical impedance spectroscopy (EIS). The EIS data in the form of a Nyquist plot (Fig. 5a) show that the Mn^{2+} doped CdS NRs have a smaller semicircle arc than the undoped CdS NRs. The as-calculated

7070 | J. Mater. Chem. A, 2023, **11**, 7066–7076

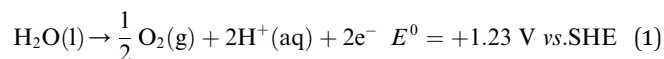This journal is © The Royal Society of Chemistry 2023

values for R_s and R_{ct} for CdS are 128.4 Ω and 5552 Ω, respectively while for Mn:CdS R_s and R_{ct} are 161.1 Ω and 1372 Ω, respectively, which shows a decreased charge transfer resistance for the CdS-based NRs upon the addition of Mn^{2+} dopants. Further dramatic reduction of charge transport resistance was obtained by Pt tipping in the Mn:CdS-Pt NRs with an extremely small semicircle arc with R_s and R_{ct} calculated to be 80.2 Ω and 499.9 Ω, respectively.

To confirm the effect of the long lifetime dopant ions on the low charge transport resistance due to the facilitated electron transport from host semiconductor NRs to Pt NP co-catalysts, we synthesized CdS NRs with Pt tips but without Mn^{2+} dopant incorporation (i.e., CdS-Pt NRs) in a control experiment (see the ESI† for the synthesis and characterization of CdS-Pt NRs). The CdS-Pt NRs have roughly the same diameter and length as the Mn:CdS-Pt NRs based on XRD and TEM analyses (Fig. S5a and b†), analogous to the CdS and Mn:CdS NRs. Compared with the EIS spectra of the CdS-Pt NRs where the calculated R_s and R_{ct} values are 92.6 Ω and 508.6 Ω, the Mn:CdS-Pt NRs have a smaller semicircle arc (Fig. 5b and S7a†) and a lower R_{ct}, which confirms that further facilitated electron transfer from Mn^{2+} dopants to Pt NPs can be achieved. In addition, the band edge emission lifetime for Mn:CdS-Pt NRs is shorter than that of CdS-Pt NRs (Fig. 3b and S6b†), showing facilitated electron transfer upon the addition of Mn^{2+} dopants with a longer PL lifetime in Mn:CdS-Pt NRs. To further confirm the enhanced electron–hole separation and charge transport in the Mn:CdS-Pt NRs, photocurrent tests were performed for the CdS-based NRs (Fig. S8†). The transient photocurrent responses increased after the incorporation of Mn^{2+} dopants in the CdS NRs, and further significant photocurrent enhancement was achieved after adding Pt NP tips on the Mn:CdS NRs, which is consistent with the reduced charge transport resistance in Mn:CdS-Pt NRs from EIS data (Fig. 5a and b).

Cyclic voltammetry (CV) was used to study the bandgap and thus the suitability of the 1D CdS NR-based photocatalysts for catalytic water reduction (Fig. 5c and S7b†). The position of the oxidative band (i.e., conduction band) can be measured by finding the onset of the current increase during the increase of the potential on the CV which occurs at ∼0.8 V vs. SHE (Fig. 5c and S7b†). Based on the bandgap calculated in a Tauc plot from the absorbance data, the position of the valence band can be obtained (Table S1†), the CdS-based NRs show a bandgap of ∼2.6 eV.

For photocatalytic H$_2$ generation by the reduction of water (gaining electrons), the half reactions and reduction potentials are shown below in eqn (1) and (2).

$$H_2O(l) \rightarrow \frac{1}{2} O_2(g) + 2H^+(aq) + 2e^- \quad E^0 = +1.23 \text{ V } vs.\text{SHE} \quad (1)$$

$$2H^+(aq) + 2e^- \rightarrow H_2(g) \; E^0 = 0.00 \text{ V } vs. \text{ SHE} \quad (2)$$

The bandgaps of each NR set-up (Fig. 5c and S7b†) are wide enough to cover the 1.23 eV needed to split water. For the Mn^{2+} doped NRs, there is an increase in the area under the CV curve at ∼0.8 V and an additional peak at ∼1.3 V and ∼1.5 V for Mn:CdS and Mn:CdS-Pt, respectively. This could be attributed to the presence of the Mn^{2+} dopants as the CV measures the available states for electrons to be added. In the presence of Pt tips, the peak at ∼1.3 V has a slight shift to ∼1.5 V which could be due to the movement of the electrons to the available Fermi level of Pt.

Photocatalytic H$_2$ generation by water splitting

Photocatalytic water splitting experiments were conducted with the as-synthesized NRs under blue light (405 nm LED) irradiation. Fig. 6a shows the catalytic performance of the 1D CdS NR-based NRs. The CdS NRs generated 120 mmol of hydrogen gas over 8 hours (9.4 mmol h^{-1} g^{-1}) with an internal quantum efficiency (IQE) of 0.5% (see the ESI† for the calculation of IQE). Mn:CdS NRs generated 149 mmol of hydrogen gas over the same period (19.8 mmol h^{-1} g^{-1}) with a greater IQE of 1.0% (Fig. S9†). A plausible reason for the increase in the photocatalytic yields from undoped NRs to the Mn^{2+} doped NRs comes from the host-to-dopant energy transfer in the Mn:CdS
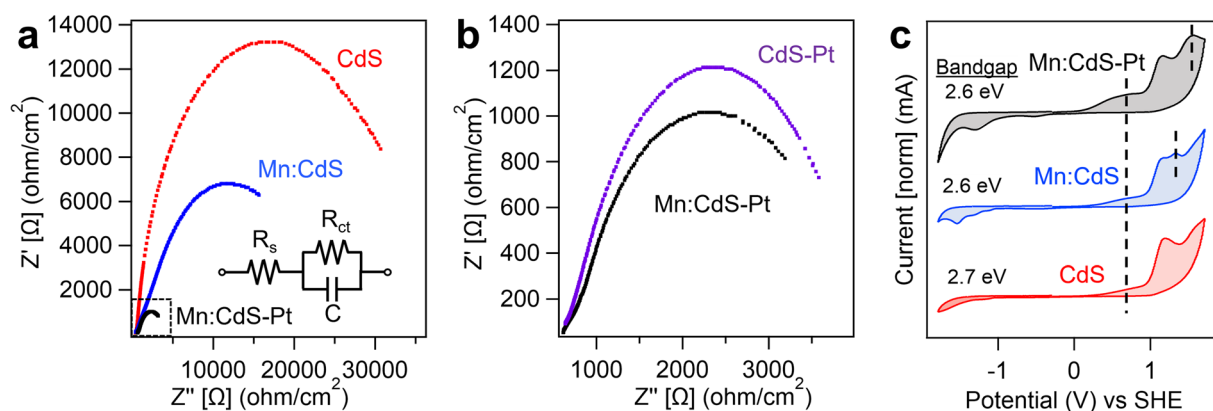

Fig. 5 (a) Electrochemical impedance spectra (Nyquist plot) of CdS, Mn:CdS, and Mn:CdS-Pt, where Z' and $-Z''$ are the virtual and real impedances, respectively. In the inset circuit diagram, R_s represents the electrolyte resistance, R_{ct} represents the charge transfer resistance, and C represents the capacitance. (b) Magnified impedance spectra area (dotted box of Fig. 4a) highlighting the decrease in impedance from CdS-Pt to Mn:CdS-Pt. (c) Normalized cyclic voltammetry spectra of CdS, Mn:CdS, and Mn:CdS-Pt NRs.
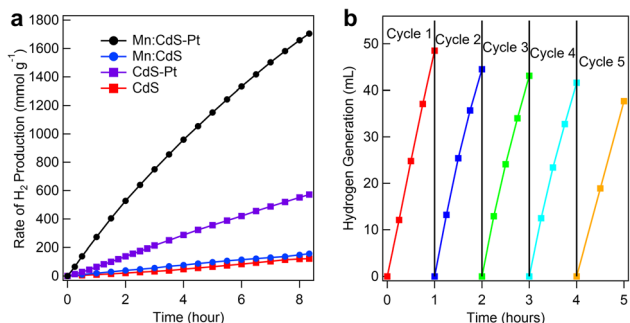
This journal is © The Royal Society of Chemistry 2023

J. Mater. Chem. A, 2023, **11**, 7066–7076 | **7071**

Fig. 6 (a) Photocatalytic performance of 1D CdS, CdS–Pt, Mn:CdS, and Mn:CdS–Pt. (b) Recycle test for the Mn:CdS–Pt photocatalytic system.

NRs, which provides excited electrons with longer lifetimes, and therefore are more accessible to take part in the photocatalytic reduction reactions. The higher photocatalytic performance of Mn:CdS NRs than CdS NRs is also consistent with the smaller charge transport resistance of Mn:CdS NRs from EIS measurements (Fig. 5b).

Upon the addition of Pt tips, the 1D Mn:CdS-Pt NRs show an excellent overall hydrogen generation with 1658 mmol of H_2 gas generated per gram of photocatalyst over 8 hours (287 mmol h^{-1} g^{-1}), with an IQE of 13.8% (Fig. S9†). The enhanced charge separation is due to the synergistic effect between long lifetime Mn^{2+} dopants and the following electron transfer to the Fermi level of Pt ($\sim$ps); electrons accumulate in the Pt NP tips for subsequent photoreduction reactions with an impressive increase in overall photocatalytic performance. The dramatically increased lifetimes of the Mn^{2+} dopants ($\sim$ms) compared to the fast exciton relaxation ($\sim$ns) of the undoped CdS NR facilities the likelihood of the excited electron to move to the Pt NPs for photocatalysis.

Recycle tests were also performed to study the stability of the photocatalysts, in which the photocatalyst was re-collected and the photocatalytic solution was remade by adding the same amount of hole scavenger at the same pH (Fig. 6b). An hour-by-hour recycling reaction using the 1D Mn:CdS-Pt photocatalyst resulted in a $\sim$94% per cycle yield of hydrogen gas from the previous hour (*i.e.*, cycle 2's yield was $\sim$94% of cycle 1), and the photocatalytic efficiency was maintained at $\sim$78% of the initial performance after five consecutive cycles. The $\sim$6% cycle-by-cycle loss could be attributed to the wash/cleaning loss of the samples as well as possible partial photodegradation[55] of the 1D Mn:CdS-Pt NRs.

To verify the sources of sample losses, ICP-OES analysis was performed to measure the concentration of Cd in the supernatant of the photocatalytic solution during the centrifugation step between cycles. The trace amount of Cd in the supernatant should be due to the wash losses of the NRs since it is impossible to recollect all NRs from centrifugation, as well as due to possible photodegradation during photocatalytic reactions. The [Cd] from collected supernatants after each cycle test is shown in Table S2,† which indicates on average $\sim$4.1% sample loss for each cycle. In addition, the transfer of the NRs to and from the glass tube could also lead to the loss of a trace amount of NR

sample (see detailed discussion in the ESI†). Therefore, the sample losses from wash, transfer, and photodegradation contribute to the slight decrease of photocatalytic performance of H_2 generation per cycle.

Furthermore, a recycle test was also performed over a 30 hour period in 10 hour cycles to assess the long-term stability of the system (Fig. S10†). The cycle-by-cycle photocatalytic yields were 93% and 83% in the second and third 10 hour cycles, respectively, indicating good reusability of the 1D photocatalysts.

Discussion

Photocatalytic mechanism of the 1D Mn:CdS-Pt NRs

Fig. 7a illustrates the host-to-dopant energy transfer and following electron transport to the Fermi level of the Pt co-catalyst in the 1D Mn:CdS-Pt NR-based photocatalysts for H_2 gas generation. The interactions between the long lifetime Mn^{2+} dopants and the Pt NP co-catalyst highlight the critical two-step charge carrier transport, *i.e.*, (1) host-to-dopant energy transfer followed by (2) electron transfer to Pt NPs, which can help prevent the fast exciton recombination ($\sim$ns) and maintain the charge separated states.

The shorter CdS PL lifetime of the Mn:CdS NRs compared to that of pristine CdS NRs (Fig. 4b) indicates the host-to-dopant energy transfer (Step 1). The following electron transfer (Step 2) from Mn:CdS to Pt is demonstrated by the decrease in PL QY after Pt NP tipping (from 6.7% to 0.9%, Fig. 4a). In addition, the Mn^{2+} dopant PL lifetime in the Mn:CdS/ZnS type I core/shell NRs also decreases after adding Pt tips due to electron transfer from Mn^{2+} dopants to Pt NP tips (Fig. 4c). Further evidence of the two successive steps is demonstrated by the reduced charge transport resistance and enhanced charge transport from CdS to Mn:CdS to Mn:CdS-Pt NRs by EIS data (Fig. 5a and b) and photocurrent results (Fig. S8†), respectively. The longer lifetime Mn^{2+} dopants can function as a bridge between the light harvesting CdS and active catalytic Pt NPs with a lower potential Fermi level (by dopant to Pt electron transfer) for enhanced charge transport, which leads to a greater water splitting efficiency.

Mn^{2+} dopant concentration-dependent photocatalytic performance

To further confirm the critical role of Mn^{2+} dopants in the Mn:CdS-Pt NRs, a control experiment of photocatalytic water splitting using undoped CdS-Pt NRs was also performed. However, the CdS-Pt NRs generated 551 mmol of H_2 gas per gram of photocatalyst over 8 hours (64 mmol h^{-1} g^{-1}) (Fig. 6a) and had an IQE of 3.1%, which is only 22.2% of the yield of Mn:CdS-Pt NRs (Fig. 6b). In this study, an optimal Mn^{2+} dopant concentration was identified as 0.9% in the as-synthesized CdS NRs.

At higher Mn^{2+} concentrations (1.4%), the photocatalytic yield fell to 81% of the ideal Mn:CdS-Pt NRs (Fig. 7b), which is due to short-range Mn–Mn interactions, leading to a concentration quenching effect as shown by a broad dipolar EPR peak without the well-resolved hyperfine peaks (Fig. S11c†).
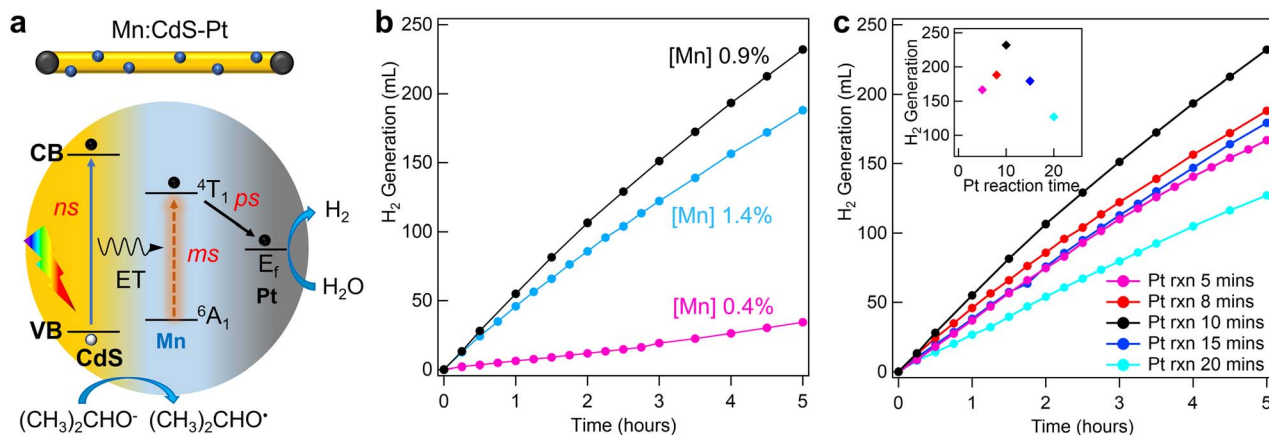
7072 | *J. Mater. Chem. A*, 2023, **11**, 7066–7076

This journal is © The Royal Society of Chemistry 2023

Fig. 7 (a) Schematic representation of the host-to-dopant energy transfer and following electron transport to the Fermi level of the Pt co-catalyst in the 1D Mn:CdS-Pt NR-based photocatalysts for H_2 gas generation by water splitting. (b) Photocatalytic performance of the Mn:CdS-Pt NRs with differing Mn^{2+} doping concentrations. (c) Pt reaction photocatalysis yields for Pt tipping reaction times of 5 to 20 minutes.

Concentration dependent quenching is common at higher doping concentrations due to the cross-relaxation between Mn–Mn coupled dopants where the dopants are closer to each other.[56,57] The concentration quenching effect can also be seen in the PL lifetime spectra of the Mn^{2+} doped NRs as the Mn^{2+} PL lifetime decreases from 4.1 to 2.9 ms when the Mn^{2+} concentration increases from 0.9% to 1.4% of the corresponding Mn:CdS/ZnS NRs (Fig. S11b and inset†). In addition, the CdS band edge PL lifetime also decreases from 3.8 to 1.4 ns as there are more Mn^{2+} ions providing an alternative relaxation pathway (Fig. S11a and inset†).

At lower Mn^{2+} concentrations, there are fewer energy transfer acceptors in the host-to-dopant energy transfer system in the Mn:CdS NRs. The lifetime of the Mn^{2+} PL stays relatively constant from 4.1 to 4.0 ms when the Mn^{2+} concentration decreases from 0.9% to 0.4% of the corresponding Mn:CdS/ZnS NRs (Fig. S11b and inset†). However, with limited Mn^{2+} dopants available at 0.4% Mn^{2+} doping concentration, fewer excited excitons can transfer their energy to Mn^{2+} dopants, and therefore, the photocatalytic yield fell to 15% of the ideal Mn:CdS-Pt NRs (Fig. 7b). This reduced host-to-dopant energy transfer at low doping concentration can be seen in the PL lifetime spectra where the band edge PL lifetime increases from 3.8 to 6.5 ns when the Mn^{2+} concentration decreases from 0.9% to 0.4% (Fig. S11a and inset†).

Size and number of Pt tip(s)-dependent photocatalytic performance

Previous work has shown that 1D NRs tipped on both ends showing an increase in their hydrogen reduction yields compared to 1D NRs tipped at only one end.[58] The Pt co-catalyst on each end of the NR allows more electrons to transfer to Pt NPs and also creates active sites on both Pt tips upon which hydrogen can adsorb onto. Once the electrons have moved to Pt, they are less likely to leave the Pt NPs and recombine within CdS as the Pt has a higher work function than the semiconductor CdS.[17] Therefore, the bridging effect from long lifetime Mn^{2+}

dopant ions is amplified in the presence of Pt (Fig. 7a) as indicated by the decreased PL QYs (Fig. 3a) and electrochemical impedance (Fig. 5a).

To control the size and number of Pt tips on 1D NRs, Pt reaction time-dependent experiments were performed. In general, the longer the Pt tipping reaction time, the more likely there will be larger Pt tips as well as Pt co-catalysts forming on both ends of the NRs while shorter Pt reaction times lead to smaller Pt tips and on only one end. In a typical 10 min Pt tipping reaction, dumbbell shaped Mn:CdS-Pt NRs with Pt tipped on each end of the NRs were obtained. When the Pt reaction time was reduced to 5 minutes, smaller Pt NPs with an average diameter of 3.2 ± 0.3 nm (Fig. S12b†) were obtained and often only tipped on one end of the NRs (Fig. S12a†). The lack of a dumbbell type NR led to lower photocatalytic performance of H_2 generation with 72% of the ideal Mn:CdS-Pt NRs (Fig. 7c and inset).

When the Pt reaction time was increased to 15 min and above, an increased Pt NP size (5.4 ± 0.4 nm under a 15 min reaction, Fig. S12 c and d†) was obtained. However, greater light scattering and absorption by the Pt co-catalyst (instead of CdS NRs) occurred which lowered the light harvesting ability of the Mn:CdS NRs and consequently, the photocatalytic performance of the NRs with a Pt tipping reaction time of 15 min was reduced to 90% of the ideal Mn:CdS-Pt NRs. Further increase of the Pt tipping reaction time results in a more dramatic decrease in the H_2 generation efficiency (Fig. 7c and inset). Therefore, the 1D Mn:CdS NRs with Pt tips on both ends with a similar diameter of the NRs are ideal for efficient light harvesting and corresponding photocatalytic water splitting.

Conclusions

We have developed new functional Mn^{2+} doped 1D CdS NRs tipped with Pt NPs (*i.e.*, Mn:CdS-Pt NRs) for photocatalytic water splitting. The energy transfer from 1D CdS host NRs to long lifetime bridging Mn^{2+} ions followed by electron transfer to the hydrophilic Pt tips of the Mn:CdS-Pt NRs limits the fast charge

recombination in the host CdS NRs, which leads to highly efficient photocatalysts for H_2 generation. EIS analysis indicates lower charge transport resistance after the incorporation of Mn^{2+} dopants with long lifetimes (~ms) inside CdS NRs due to the host-to-dopant energy transfer. Further significant decrease of impedance after the tipped with Pt NPs occurs as a result of electron transfer from the NRs to the metal NPs. Our rationally designed 1D Mn:CdS-Pt NR photocatalysts take advantage of the long lifetime of Mn^{2+} dopants (~ms) for efficient charge separation and electron transfer, exhibiting ~4.5 times greater photocatalytic yields of H_2 generation from water splitting than undoped CdS-Pt NRs. The functional 1D photocatalysts by introducing dopants as charge transport bridges provide new opportunities for facilitated electron transfer of high performance photocatalysts.

Conflicts of interest

There are no conflicts to declare.

Acknowledgements

References

1 P. P. Edwards, V. L. Kuznetsov and W. I. David, Hydrogen energy, *Philos. Trans. R. Soc., A*, 2007, **365**(1853), 1043–1056.

2 K. Wu and T. Lian, Quantum confined colloidal nanorod heterostructures for solar-to-fuel conversion, *Chem. Soc. Rev.*, 2016, **45**(14), 3781–3810.

3 J. Yu, Y. Yu, P. Zhou, W. Xiao and B. Cheng, Morphology-dependent photocatalytic H_2-production activity of CdS, *Appl. Catal., B*, 2014, **156–157**, 184–191.

4 K. Kim, M.-J. Kim, S.-I. Kim and J.-H. Jang, Towards Visible Light Hydrogen Generation: Quantum Dot-Sensitization *via* Efficient Light Harvesting of Hybrid-TiO_2, *Sci. Rep.*, 2013, **3**(1), 3330.

5 Z.-J. Li, X.-B. Fan, X.-B. Li, J.-X. Li, F. Zhan, Y. Tao, X. Zhang, Q.-Y. Kong, N.-J. Zhao, J.-P. Zhang, C. Ye, Y.-J. Gao, X.-Z. Wang, Q.-Y. Meng, K. Feng, B. Chen, C.-H. Tung and L.-Z. Wu, Direct synthesis of all-inorganic heterostructured CdSe/CdS QDs in aqueous solution for improved photocatalytic hydrogen generation, *J. Mater. Chem. A*, 2017, **5**(21), 10365–10373.

6 Z.-J. Li, J.-J. Wang, X.-B. Li, X.-B. Fan, Q.-Y. Meng, K. Feng, B. Chen, C.-H. Tung and L.-Z. Wu, An Exceptional Artificial Photocatalyst, Ni_h-CdSe/CdS Core/Shell Hybrid, Made *In Situ* from CdSe Quantum Dots and Nickel Salts for Efficient Hydrogen Evolution, *Adv. Mater.*, 2013, **25**(45), 6613–6618.

7 R. Trevisan, P. Rodenas, V. Gonzalez-Pedro, C. Sima, R. S. Sanchez, E. M. Barea, I. Mora-Sero, F. Fabregat-Santiago and S. Gimenez, Harnessing Infrared Photons for Photoelectrochemical Hydrogen Generation. A PbS Quantum Dot Based "Quasi-Artificial Leaf", *J. Phys. Chem. Lett.*, 2013, **4**(1), 141–146.

8 L. Yu, W. Chen, D. Li, J. Wang, Y. Shao, M. He, P. Wang and X. Zheng, Inhibition of photocorrosion and photoactivity enhancement for ZnO *via* specific hollow ZnO core/ZnS shell structure, *Appl. Catal., B*, 2015, **164**, 453–461.

9 A. Meng, B. Zhu, B. Zhong, L. Zhang and B. Cheng, Direct Z-scheme TiO_2/CdS hierarchical photocatalyst for enhanced photocatalytic H_2-production activity, *Appl. Surf. Sci.*, 2017, **422**, 518–527.

10 J. Yuan, J. Wen, Q. Gao, S. Chen, J. Li, X. Li and Y. Fang, Amorphous Co_3O_4 modified CdS nanorods with enhanced visible-light photocatalytic H_2-production activity, *Dalton Trans.*, 2015, **44**(4), 1680–1689.

11 J. A. Nasir, Z. u. Rehman, S. N. A. Shah, A. Khan, I. S. Butler and C. R. A. Catlow, Recent developments and perspectives in CdS-based photocatalysts for water splitting, *J. Mater. Chem. A*, 2020, **8**(40), 20752–20780.

12 K. Wu, Z. Chen, H. Lv, H. Zhu, C. L. Hill and T. Lian, Hole removal rate limits photodriven H_2 generation efficiency in CdS-Pt and CdSe/CdS-Pt semiconductor nanorod-metal tip heterostructures, *J. Am. Chem. Soc.*, 2014, **136**(21), 7708–7716.

13 S. Corby, R. R. Rao, L. Steier and J. R. Durrant, The kinetics of metal oxide photoanodes from charge generation to catalysis, *Nat. Rev. Mater.*, 2021, **6**(12), 1136–1155.

14 J. Wang, L. Xiong, Y. Bai, Z. Chen, Q. Zheng, Y. Shi, C. Zhang, G. Jiang and Z. Li, Mn-Doped Perovskite Nanocrystals for Photocatalytic CO_2 Reduction: Insight into the Role of the Charge Carriers with Prolonged Lifetime, *Sol. RRL*, 2022, **6**(8), 2200294.

15 L. Ge, F. Zuo, J. Liu, Q. Ma, C. Wang, D. Sun, L. Bartels and P. Feng, Synthesis and Efficient Visible Light Photocatalytic Hydrogen Evolution of Polymeric g-C_3N_4 Coupled with CdS Quantum Dots, *J. Phys. Chem. C*, 2012, **116**(25), 13708–13714.

16 J. S. Jang, U. A. Joshi and J. S. Lee, Solvothermal Synthesis of CdS Nanowires for Photocatalytic Hydrogen and Electricity Production, *J. Phys. Chem. C*, 2007, **111**(35), 13280–13287.

17 Q. Li, F. Zhao, C. Qu, Q. Shang, Z. Xu, L. Yu, J. R. McBride and T. Lian, Two-Dimensional Morphology Enhances Light-Driven H_2 Generation Efficiency in CdS Nanoplatelet-Pt Heterostructures, *J. Am. Chem. Soc.*, 2018, **140**(37), 11726–11734.

18 M. Muruganandham, Y. Kusumoto, C. Okamoto, A. Muruganandham, M. Abdulla-Al-Mamun and B. Ahmmad, Mineralizer-Assisted Shape-Controlled Synthesis, Characterization, and Photocatalytic Evaluation of CdS Microcrystals, *J. Phys. Chem. C*, 2009, **113**(45), 19506–19517.

19 N. Bao, L. Shen, T. Takata and K. Domen, Self-Templated Synthesis of Nanoporous CdS Nanostructures for Highly Efficient Photocatalytic Hydrogen Production under Visible Light, *Chem. Mater.*, 2008, **20**(1), 110–117.

7074 | *J. Mater. Chem. A*, 2023, **11**, 7066–7076

This journal is © The Royal Society of Chemistry 2023

20 B. T. Diroll, A. Koschitzky and C. B. Murray, Tunable Optical Anisotropy of Seeded CdSe/CdS Nanorods, *J. Phys. Chem. Lett.*, 2014, **5**(1), 85–91.

21 Y. Liu, W. Yang, Q. Chen, D. A. Cullen, Z. Xie and T. Lian, Pt Particle Size Affects Both the Charge Separation and Water Reduction Efficiencies of CdS–Pt Nanorod Photocatalysts for Light Driven H_2 Generation, *J. Am. Chem. Soc.*, 2022, **144**(6), 2705–2715.

22 K. Wu, H. Zhu and T. Lian, Ultrafast exciton dynamics and light-driven H_2 evolution in colloidal semiconductor nanorods and Pt-tipped nanorods, *Acc. Chem. Res.*, 2015, **48**(3), 851–859.

23 M. Berr, A. Vaneski, A. S. Susha, J. Rodríguez-Fernández, M. Döblinger, F. Jäckel, A. L. Rogach and J. Feldmann, Colloidal CdS nanorods decorated with subnanometer sized Pt clusters for photocatalytic hydrogen generation, *Appl. Phys. Lett.*, 2010, **97**(9), 093108.

24 K. Chen, S.-J. Ding, S. Ma, W. Wang, S. Liang, L. Zhou and Q.-Q. Wang, Enhancing Photocatalytic Activity of Au-Capped CdS–PbS Heterooctahedrons by Morphology Control, *J. Phys. Chem. C*, 2020, **124**(14), 7938–7945.

25 J. Hao, H. Liu, K. Wang, X. W. Sun, J.-P. Delville and M.-H. Delville, Hole Scavenging and Electron–Hole Pair Photoproduction Rate: Two Mandatory Key Factors to Control Single-Tip Au–CdSe/CdS Nanoheterodimers, *ACS Nano*, 2021, **15**(9), 15328–15341.

26 H. Wang, W. Chen, J. Zhang, C. Huang and L. Mao, Nickel nanoparticles modified CdS – A potential photocatalyst for hydrogen production through water splitting under visible light irradiation, *Int. J. Hydrogen Energy*, 2015, **40**(1), 340–345.

27 B. Zhang, C. Chen, J. Liu, W. Qiao, J. Zhao, J. Yang, Y. Yu, S. Chen and Y. Qin, Simultaneous Ni nanoparticles decoration and Ni doping of CdS nanorods for synergistically promoting photocatalytic H_2 evolution, *Appl. Surf. Sci.*, 2020, **508**, 144869.

28 S. Saeed, H. Siddique, R. Dai, J. Wang, A. Ali, C. Gao, X. Tao, Z. Wang, Z. Ding and Z. Zhang, Enhanced PEC Water Splitting Performance of Silver Nanoparticle-Coated CdS Nanowire Photoanodes: The Role of Silver Deposition, *J. Phys. Chem. C*, 2021, **125**(14), 7542–7551.

29 H. Yan, J. Yang, G. Ma, G. Wu, X. Zong, Z. Lei, J. Shi and C. Li, Visible-light-driven hydrogen production with extremely high quantum efficiency on Pt–PdS/CdS photocatalyst, *J. Catal.*, 2009, **266**(2), 165–168.

30 A. Ye, W. Fan, Q. Zhang, W. Deng and Y. Wang, CdS–graphene and CdS–CNT nanocomposites as visible-light photocatalysts for hydrogen evolution and organic dye degradation, *Catal. Sci. Technol.*, 2012, **2**(5), 969–978.

31 J. Wang, Y. Li, Q. Shen, T. Izuishi, Z. Pan, K. Zhao and X. Zhong, Mn doped quantum dot sensitized solar cells with power conversion efficiency exceeding 9, *J. Mater. Chem. A*, 2016, **4**(3), 877–886.

32 B. He, R. Liu, J. Ren, C. Tang, Y. Zhong and Y. Hu, One-Step Solvothermal Synthesis of Petalous Carbon-Coated Cu^+-Doped CdS Nanocomposites with Enhanced Photocatalytic Hydrogen Production, *Langmuir*, 2017, **33**(27), 6719–6726.

33 Y. Dong, J. Choi, H.-K. Jeong and D. H. Son, Hot Electrons Generated from Doped Quantum Dots *via* Upconversion of Excitons to Hot Charge Carriers for Enhanced Photocatalysis, *J. Am. Chem. Soc.*, 2015, **137**(16), 5549–5554.

34 Y. Dong, D. Parobek, D. Rossi and D. H. Son, Photoemission of Energetic Hot Electrons Produced *via* Up-Conversion in Doped Quantum Dots, *Nano Lett.*, 2016, **16**(11), 7270–7275.

35 D.-Y. Jo, D. Kim, J.-H. Kim, H. Chae, H. J. Seo, Y. R. Do and H. Yang, Tunable White Fluorescent Copper Gallium Sulfide Quantum Dots Enabled by Mn Doping, *ACS Appl. Mater. Interfaces*, 2016, **8**(19), 12291–12297.

36 J. Dehnel, Y. Barak, I. Meir, A. K. Budniak, A. P. Nagvenkar, D. R. Gamelin and E. Lifshitz, Insight into the Spin Properties in Undoped and Mn-Doped CdSe/CdS-Seeded Nanorods by Optically Detected Magnetic Resonance, *ACS Nano*, 2020, **14**(10), 13478–13490.

37 Y. Yang, O. Chen, A. Angerhofer and Y. C. Cao, On Doping CdS/ZnS Core/Shell Nanocrystals with Mn, *J. Am. Chem. Soc.*, 2008, **130**(46), 15649–15661.

38 M. Liu, Y. Du, L. Ma, D. Jing and L. Guo, Manganese doped cadmium sulfide nanocrystal for hydrogen production from water under visible light, *Int. J. Hydrogen Energy*, 2012, **37**(1), 730–736.

39 Z.-J. Li, S. Li, A. H. Davis, E. Hofman, G. Leem and W. Zheng, Enhanced singlet oxygen generation by hybrid Mn-doped nanocomposites for selective photo-oxidation of benzylic alcohols, *Nano Res.*, 2020, **13**(6), 1668–1676.

40 A. E. Saunders, A. Ghezelbash, P. Sood and B. A. Korgel, Synthesis of High Aspect Ratio Quantum-Size CdS Nanorods and Their Surface-Dependent Photoluminescence, *Langmuir*, 2008, **24**(16), 9043–9049.

41 S. E. Habas, P. Yang and T. Mokari, Selective Growth of Metal and Binary Metal Tips on CdS Nanorods, *J. Am. Chem. Soc.*, 2008, **130**(11), 3294–3295.

42 Y.-N. Xu and W. Y. Ching, Electronic, optical, and structural properties of some wurtzite crystals, *Phys. Rev. B*, 1993, **48**(7), 4335–4351.

43 S. Mardix, E. Alexander, O. Brafman and I. T. Steinberger, Polytype families in zinc sulphide crystals, *Acta Crystallogr.*, 1967, **22**(6), 808–812.

44 J. Tian, L. Lv, C. Fei, Y. Wang, X. Liu and G. Cao, A highly efficient (>6%) $Cd_{1-x}Mn_xSe$ quantum dot sensitized solar cell, *J. Mater. Chem. A*, 2014, **2**(46), 19653–19659.

45 A. J. Yost, T. K. Ekanayaka, G. Gurung, G. Rimal, S. Horoz, J. Tang, T. Paudel and T. Chien, Influence of the Cation on the Surface Electronic Band Structure and Magnetic Properties of Mn:ZnS and Mn:CdS Quantum Dot Thin Films, *J. Phys. Chem. C*, 2019, **123**(40), 24890–24898.

46 D. You, B. Pan, Y. He, X. Wang and W. Su, Enhanced visible light photocatalytic H_2 evolution over CeO_2 loaded with Pt and CdS, *Res. Chem. Intermed.*, 2017, **43**(9), 5103–5112.

47 S. Liu, Z. Guo, X. Qian, J. Zhang, J. Liu and J. Lin, Sonochemical deposition of ultrafine metallic Pt nanoparticles on CdS for efficient photocatalytic hydrogen evolution, *Sustainable Energy Fuels*, 2019, **3**(4), 1048–1054.

48 H. Park, Y. K. Kim and W. Choi, Reversing CdS Preparation Order and Its Effects on Photocatalytic Hydrogen Production

This journal is © The Royal Society of Chemistry 2023

J. Mater. Chem. A, 2023, **11**, 7066–7076 | **7075**

of CdS/Pt-TiO$_2$ Hybrids Under Visible Light, *J. Phys. Chem. C*, 2011, **115**(13), 6141–6148.

49 A. H. Davis, E. Hofman, K. Chen, Z.-J. Li, A. Khammang, H. Zamani, J. M. Franck, M. M. Maye, R. W. Meulenberg and W. Zheng, Exciton Energy Shifts and Tunable Dopant Emission in Manganese-Doped Two-Dimensional CdS/ZnS Core/Shell Nanoplatelets, *Chem. Mater.*, 2019, **31**(7), 2516–2523.

50 L. R. Bradshaw, A. Hauser, E. J. McLaurin and D. R. Gamelin, Luminescence Saturation *via* Mn^{2+}–Exciton Cross Relaxation in Colloidal Doped Semiconductor Nanocrystals, *J. Phys. Chem. C*, 2012, **116**(16), 9300–9310.

51 X. Cao, X. Zheng, J. Tian, C. Jin, K. Ke and R. Yang, Cobalt Sulfide Embedded in Porous Nitrogen-doped Carbon as a Bifunctional Electrocatalyst for Oxygen Reduction and Evolution Reactions, *Electrochim. Acta*, 2016, **191**, 776–783.

52 E. Hofman, A. Khammang, J. T. Wright, Z.-J. Li, P. F. McLaughlin, A. H. Davis, J. M. Franck, A. Chakraborty, R. W. Meulenberg and W. Zheng, Decoupling and Coupling of the Host–Dopant Interaction by Manipulating Dopant Movement in Core/Shell Quantum Dots, *J. Phys. Chem. Lett.*, 2020, **11**(15), 5992–5999.

53 W. Zheng, Z. Wang, J. Van Tol, N. S. Dalal and G. F. Strouse, Alloy Formation at the Tetrapod Core/Arm Interface, *Nano Lett.*, 2012, **12**(6), 3132–3137.

54 W. Zheng, Z. Wang, J. Wright, B. Goundie, N. S. Dalal, R. W. Meulenberg and G. F. Strouse, Probing the Local Site Environments in Mn:CdSe Quantum Dots, *J. Phys. Chem. C*, 2011, **115**(47), 23305–23314.

55 P. Kalisman, Y. Kauffmann and L. Amirav, Photochemical oxidation on nanorod photocatalysts, *J. Mater. Chem. A*, 2015, **3**(7), 3261–3265.

56 Z. Wang and A. Meijerink, Concentration Quenching in Upconversion Nanocrystals, *J. Phys. Chem. C Nanomater. Interfaces*, 2018, **122**(45), 26298–26306.

57 J. Cao, J. Yang, Y. Zhang, L. Yang, Y. Wang, M. Wei, Y. Liu, M. Gao, X. Liu and Z. Xie, Optimized doping concentration of manganese in zinc sulfide nanoparticles for yellow-orange light emission, *J. Alloys Compd.*, 2009, **486**(1–2), 890–894.

58 J. Y. Choi, W.-W. Park, B. Park, S. Sul, O.-H. Kwon and H. Song, Optimal Length of Hybrid Metal–Semiconductor Nanorods for Photocatalytic Hydrogen Generation, *ACS Catal.*, 2021, **11**(21), 13303–13311.